ACS SyntheticBiology

pubs.acs.org/synthbio

Research Article

Construction and Application of a High-Throughput *In Vivo* Screening Platform for the Evolution of Nitrile Metabolism-Related Enzymes Based on a Desensitized Repressive Biosensor

Laichuang Han, Xinyue Liu, Zhongyi Cheng, Wenjing Cui, Junling Guo, Jian Yin, and Zhemin Zhou*

Cite This: *ACS Synth. Biol.* 2022, 11, 1577−1587

Read Online

ACCESS | Metrics & More | Article Recommendations | Supporting Information

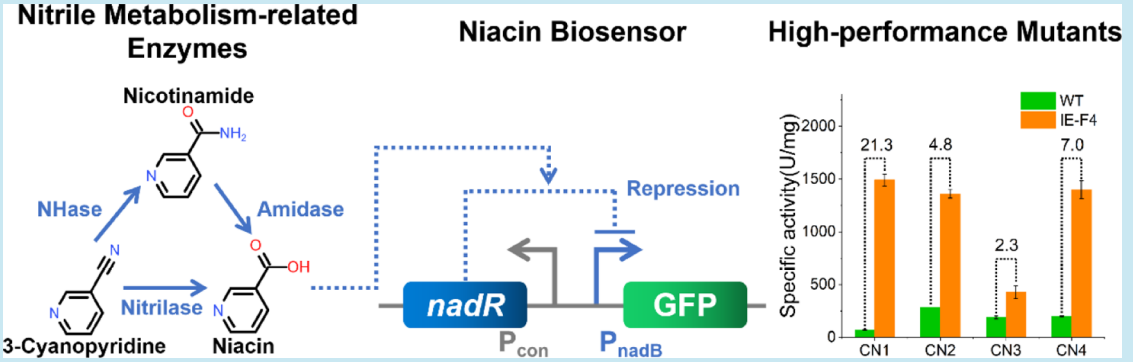

ABSTRACT: Transcription factor (TF)-based biosensors are expected to serve as powerful tools for the high-throughput screening of biocatalytic systems; however, most of them respond to ligands in a narrow concentration range, which limits their application. In this study, we constructed a heterogenous niacin biosensor using the repressive TF BsNadR and its target promoters from *Bacillus subtilis*. The fine-tunable output of the niacin biosensor was expanded to a wide range of niacin concentrations (0−50 mM) through desensitization engineering, which was suitable for the accurate identification of differences in enzyme activity. Structural mechanism analysis indicated that weakening the affinity of BsNadR with the ligand niacin and with DNA alters its regulatory properties. Based on the desensitized niacin biosensor, a high-throughput *in vivo* screening platform was developed for evolving nitrile metabolism-related enzymes. The evolved nitrilase, amidase, and nitrile hydratase with 6.6-, 2.1-, and 21.3-fold improvements in activity were achieved, respectively. In addition, these mutants also exhibited elevated activity toward other cognate substrates, indicating the broad applicability of the screening platform. This study not only provided a universal high-throughput screening platform for different nitrile metabolism-related enzymes but also demonstrated the advantages of repressive biosensors and the vital role of desensitization engineering of the TF in the development of high-throughput screening platforms for enzymes.

KEYWORDS: *biosensor, repressive transcription factor, high-throughput screening, directed evolution, nitrile metabolism-related enzymes*

INTRODUCTION

Enzymes are important biocatalysts that are increasingly replacing chemical catalysts in biochemical reactions, pharmaceutical intermediate synthesis, and food and feed preparation due to their mild reaction conditions, environmentally friendly properties, and high catalytic efficiency. Because of the rapid expansion of enzyme application scenarios, natural enzymes often need to be improved to optimize their properties, such as catalytic activity, thermostability, and tolerance to organic solvents, in non-native environments. Directed evolution has been established to be a powerful technique to enhance catalytic activities of enzymes or develop novel enzymes for catalyzing unnatural reactions.[1,2] More importantly, directed evolution offers the possibility to enhance the catalytic activity of enzymes through "undesignable routes," such as reshaping global dynamical networks and energy landscapes.[3,4] In directed evolution, the target mutants are always sorted out from libraries with different scales generated by error-prone PCR (EP-PCR), DNA shuffling, or site saturation mutagenesis.[5−7] For instance, it is conceivable that the combined saturation mutagenesis in two residues would theoretically contain 4×10^2 mutations, while merely five residues would amount to 3.2×10^6. Therefore, it would be an extremely time- and labor-consuming process without a convenient high-throughput screening technique.

Received: December 28, 2021
Published: March 10, 2022

https://doi.org/10.1021/acssynbio.1c00642
ACS Synth. Biol. 2022, 11, 1577−1587

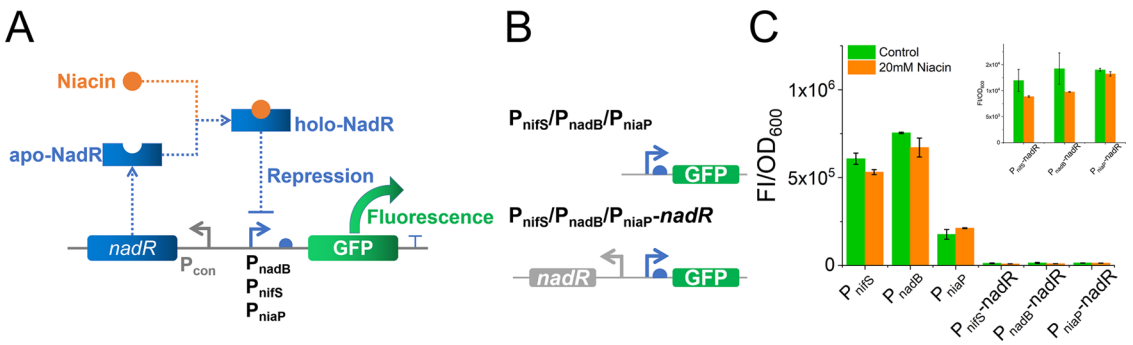

Figure 1. Design and verification of the NAsensor. (A) Schematic diagram of the NAsensor. BsNadR was expressed by a constitutive promoter (P_{con}). After binding niacin, BsNadR repressed the activity of three candidate promoters (P_{nadB}, P_{nifS}, and P_{niaP}), establishing the correlation between the niacin concentration and the GFP expression strength. (B) Two forms of GFP expression cassettes. One was the constitutive GFP expression by candidate promoters, and another was introducing BsNadR to regulate the activity of candidate promoters. (C) Verification of the NAsensor. Control means culture in LB without chemical addition. FI, fluorescence intensity.

Isolation of the evolved enzymes is often carried out by high-throughput screening platforms based on physical or chemical reactions *in vitro*.[8−10] In such a screening process, multiple steps including protein expression, cell fragmentation, and *in vitro* enzymatic activity assays need to be performed sequentially, which is quite inconvenient. Therefore, a high-throughput screening platform allowing the *in vivo* identification of enzymatic activity is expected to accelerate the evolution of enzymes. A biosensor is an ideal connector between enzyme activity and the cellular phenotype, allowing direct *in vivo* ultrahigh-throughput characterization of enzyme activity.[11] Transcription factors (TFs) regulate gene expression over a greater dynamic range,[12] and they have been increasingly developed for protein engineering, metabolic engineering, and synthetic biology.[13−16] However, limited by the inherent shortcomings of natural TFs, they often need to be adaptively evolved before meeting application needs.[17] For instance, natural TFs are susceptible to full activation by a trace concentration of inducers (usually less than 1 mM), but the progressive reporter gene expression is difficult to achieve.[18−20] Accordingly, in some cases, natural TFs need to be adaptively evolved for wider operating ranges because the strong correlation between the ligand concentration and the signal output is vital for enzyme screening.

NadR from *Bacillus subtilis* (BsNadR), also referred to as NiaR or YrxA, is a repressive TF involved in nicotinamide adenine dinucleotide synthesis and represses the transcription of six genes (*nadB*, *nadC*, *nadA*, *nadR*, *nifS*, and *niaP*) in response to niacin concentration (Figure S1).[21,22] Niacin is a 3-cyanopyridine metabolite produced by the catalytic activity of nitrilase, amidase, and nitrile hydratase (NHase). These enzymes are ideal biocatalysts that convert low-cost nitrile into high-value-added bulk chemicals and pharmaceutical intermediates of amides and acids, such as acrylamide, L-2-aminobutyramide, nicotinamide, niacin, and (*R*)-(−)-mandelic acid.[23−25] However, to date, only acrylamide and nicotinamide generated from acrylonitrile and 3-cyanopyridine, respectively, by NHase-mediated catalysis have been applied in industrial products. Other products have not been successfully optimized due to the low activity of nitrilase and amidase, as well as the low activity of NHase toward other nitriles.[25] Evolution of these enzymes has progressed at a slow pace due to the lack of a high-throughput screening method. Although chromogenic reagents and pH indicators were employed earlier to measure the formation of carboxyl groups and ammonia to monitor the hydrolase activity of nitrilase,[26−29] these methods required setting up of individual reactions and further processing of the catalytic products, thus making large throughputs difficult to achieve.

In this study, a high-throughput automatic *in vivo* screening platform for nitrilase, amidase, and NHase was constructed based on a niacin biosensor (NAsensor). The NAsensor was constructed according to the BsNadR regulation model using a green fluorescent protein (GFP) as a reporter and further developed. The NAsensor responded to a wide range of niacin concentrations (0−50 mM), and exhibited a gradient signal output. The analysis of the developed NAsensor indicated that the response to a wide range of niacin concentrations was caused by weakening of the binding force of BsNadR with niacin and DNA. A high-throughput *in vivo* screening platform for nitrilase and amidase was constructed based on the developed NAsensor. Furthermore, the high-throughput screening platform expanded for NHase screening with the introduction of a nicotinamide conversion module. Using the high-throughput screening platform, three mutants of nitrilase, amidase, and nitrile hydratase, with 6.6-, 2.1-, and 21.3-fold improvements in activity, respectively, were directly isolated. Notably, activities of the isolated enzymes toward other substrates were also improved.

RESULTS AND DISCUSSION

Design and Construction of a Heterologous Orthogonal Niacin Biosensor. Heterologous biological parts are able to construct regulation systems, such as the heterologous utilization of sigma factors from *B. subtilis* in *Escherichia coli*.[30] On the one hand, these parts can work across hosts; on the other hand, their specificity in binding sequences to DNA ensures high orthogonality with the host's own gene regulatory network. This is important for the stable existence and function of the biosensor. The repressive NAsensor in *E. coli* is illustrated in Figure 1A. In this system, GFP was expressed under the control of three candidate promoters (P_{nadB}, P_{nifS}, and P_{niaP}). Theoretically, the constitutively expressed BsNadR would repress the activity of the target promoter when bound to niacin, with higher concentrations resulting in higher repression ratios.

The functions of the three candidate promoters were first determined in the three systems lacking BsNadR (Figure 1B). Fluorescence detection showed that the candidate promoters constitutively expressed GFP. P_{nadB} exhibited the highest

https://doi.org/10.1021/acssynbio.1c00642
ACS Synth. Biol. 2022, 11, 1577−1587

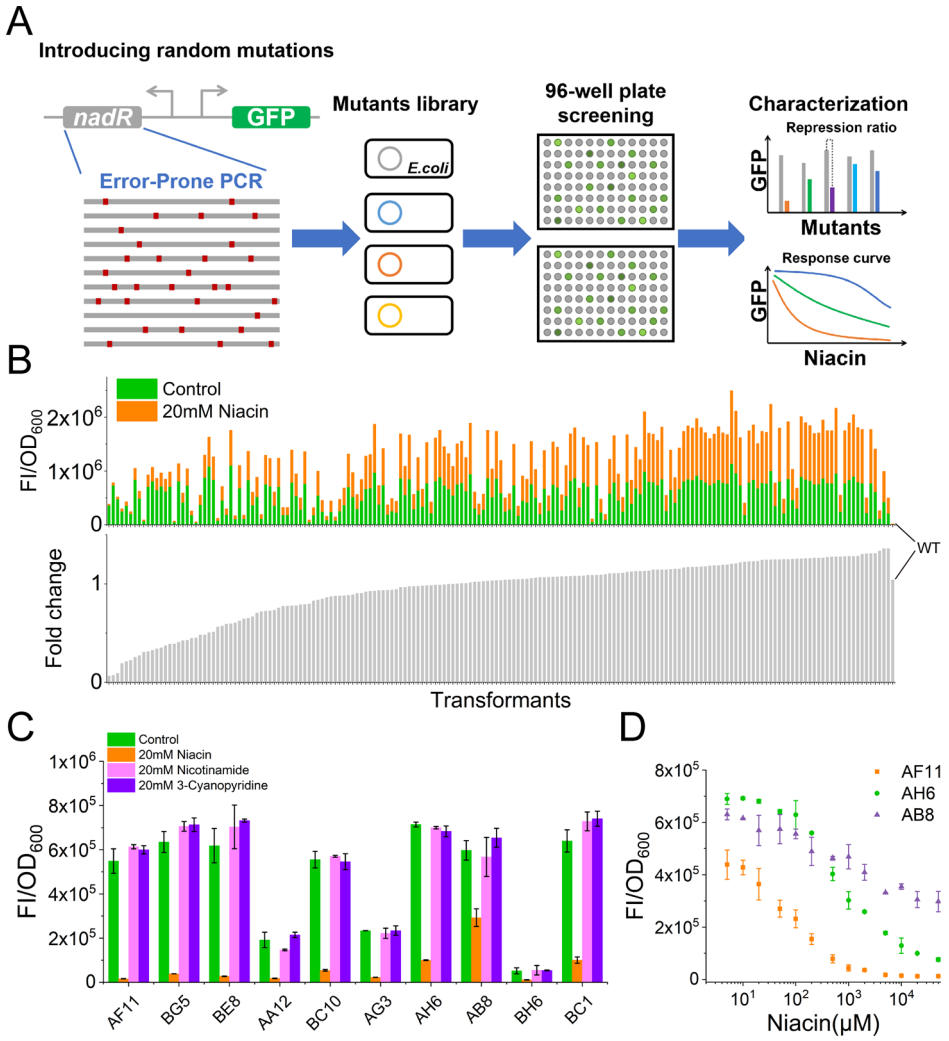

Figure 2. Desensitization engineering of BsNadR. (A) Procedure for screening desensitized BsNadR by EP-PCR. (B) Screening of BsNadR mutants. Transformants with BsNadR mutants were individually cultured with or without (control) of 20 mM niacin, and the GFP expression was determined and shown by the stacked bar plot. Transformants were ranked according to the fold change, which means the ratio of fluorescence intensity when niacin was added to that of control. (C) Fluorescence intensity determination of the top 10 BsNadR mutants. (D) Fluorescence intensity determination of AF11, AH6, and AB8 under various concentrations of niacin. The x-axis was logarithmic (log 10). FI, fluorescence intensity.

activity, with no significant impact on the GFP expression observed as a consequence of adding niacin (Figure 1C). Subsequently, the BsNadR expression cassette was introduced into the plasmid to establish the correlation between promoter activity and the niacin concentration (Figure 1C). However, GFP expression was almost completely suppressed even in the control group. This may be explained by BsNadR being oversensitive to niacin, such that even trace amounts of metabolically synthesized niacin result in extremely strong repressive activity. To verify this hypothesis, we characterized the P_{nadB}-based NAsensor in the *pncA*-deficient strain, in which the synthesis of endogenous niacin would theoretically be impaired. As expected, the function of the NAsensor has been slightly improved in the *pncA*-deficient strain (Figure S2), which supports our hypothesis. In fact, ultra-sensitivity is a characteristic of many natural regulators, which prevents artificial genetic circuits built on natural regulators from working as expected.[31,32] Therefore, desensitization of BsNadR was essential to modify the response of this regulatory system to make it functional at the desired niacin concentration.

Modulating the Response Range of the NAsensor Through TF Desensitization Engineering. As a TF, the ligand-induced allosterism of BsNadR is quite complex. It is very difficult to tune the regulatory property of BsNadR by the rational design. Therefore, a desensitization engineering strategy of BsNadR based on EP-PCR was proposed. As shown in Figure 2A, mutations with random position and number were first introduced into BsNadR by EP-PCR. The plasmids of the mutant library were constructed by seamless cloning *in vitro* and then transformed into *E. coli* JM109. The transformed cells were plated onto LB plates without niacin addition and then pre-screened under the blue light on plates. Single colonies with high fluorescence were inoculated into 96-well plates and cultured in the LB with or without niacin. The recombinant strains in which GFP expression can be efficiently suppressed by niacin were further characterized in test tubes. Finally, the desensitized mutants of BsNadR with different operating ranges were obtained.

Since the promoter P_{nadB} exhibited the highest activity, which resulted in a greater dynamic range of GFP expression in

https://doi.org/10.1021/acssynbio.1c00642
ACS Synth. Biol. 2022, 11, 1577−1587

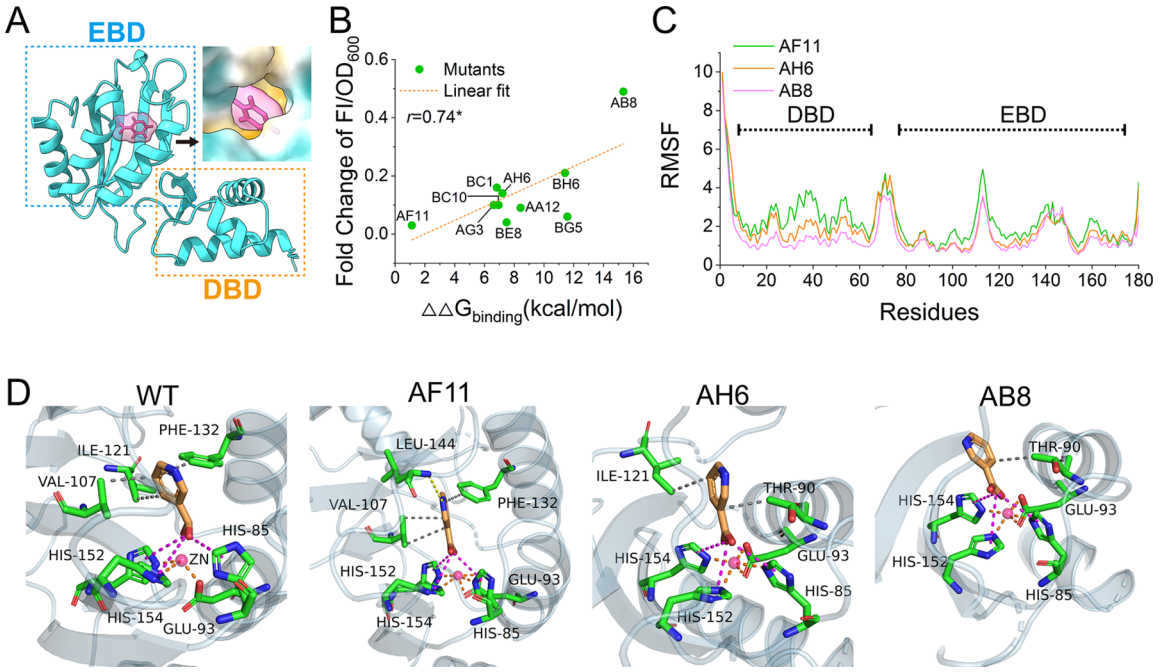

Figure 3. Structural analysis of BsNadR mutants. (A) Overview of the complex structure of BsNadR-bound niacin. The ligand niacin is shown as a stick colored by hot pink. (B) The correlations between the free energy of ligand binding ($\Delta\Delta G_{binding}$) and the fold change of GFP expression repressed by 20 mM niacin. The correlation was determined using Pearson's correlation, and the significant difference was analyzed using Student's *t*-test. * The significant difference was at $P < 0.01$ level. (C) RMSF analysis of three BsNadR mutant-bound niacin. The region of DBD and EBD was labeled in the graph. (D) Structural analysis of niacin binding in WT and three mutants. The yellow, magenta, orange, and gray dashed lines indicate a hydrogen bond, a salt bridge, metal complexation, and hydrophobic interaction, respectively.

the NAsensor, the plasmid containing P_{nadB} and *nadR* genes was used as the template to achieve desensitization of the NAsensor. A total of 180 transformants with higher GFP expression were selected from the mutant library, and their GFP expression levels without and with niacin were determined (Figure 2B). Most of them exhibited high GFP expression without the addition of niacin, which was significantly different from that observed in the presence of niacin for each transformant. The candidate transformants were further ranked according to the fold change in GFP expression due to repression, and the top 10 transformants were repeatedly validated (Table S3).

The GFP expression in the mutants was repressed to different degrees by niacin, suggesting that the mutations of BsNadR modulated the response of the NAsensor (Figure 2C). Moreover, the addition of nicotinamide and 3-cyanopyridine showed no obvious repression of GFP expression, indicating that the mutants were highly selective for niacin (Figure 2C). Three of the mutants, AF11, AH6, and AB8, which exhibited high, medium, and low responses, respectively, to niacin, were selected for further characterization. The GFP expression profiles of these mutants varied at different niacin concentrations (Figure 2D). Among these three mutants, AF11 was the most sensitive to niacin, the effect of niacin on AB8 was the weakest, and AH6 responded to niacin over the widest concentration range by presenting a gradient of GFP expression over a range of 0−50 mM niacin (Figure 2D), and hence, it was best suited for screening enzyme activity.

Structural Mechanisms of BsNadR Mutants with Different Regulatory Properties. To explore the impact of mutations on the regulatory properties, the 3D structure of BsNadR was built using homology modeling (Figure S3). The protein−ligand complex structure was further obtained using molecular docking (Figure 3A). BsNadR consists of an N-terminal DNA-binding domain (DBD) and a C-terminal effector-binding domain (EBD). EBD binds with niacin in a hydrophobic ligand-binding pocket (Figure 3A). The affinity of TFs for ligands is one of the fundamental molecular mechanisms responsible for different sensitivities.[17] The NAsensor mutants characterized above exhibited different degrees of suppression of GFP expression at similar niacin concentrations (Figure 2C), thereby implying that the mutations endowed BsNadR with variable sensitivities to niacin binding. To evaluate this supposition, the affinity of BsNadR mutants for niacin was assessed using the free energy perturbation/Hamiltonian replica exchange molecular dynamics (FEP/HREMD) method.[33] Results indicated that each BsNadR mutant bound niacin with a different binding free energy, which was significantly higher than that of the wild type (Figure S4). A correlation between the fold changes in GFP expression and the binding free energy ($\Delta\Delta G$) was analyzed. As shown in Figure 3B, a strong positive correlation was observed between the two factors, demonstrating that the mutations modulated the affinity of BsNadR for niacin, thereby altering the response of the NAsensor. Notably, WT and AF11 do not differ significantly in binding free energy to the ligand, but they differ significantly in their regulation of GFP expression in response to niacin. This phenomenon implies that structural changes in DBD also affect the regulatory properties of BsNadR, not just the EBD.

MD simulations were applied to AF11, AH6, and AB8 to further resolve differences in structural dynamics characteristics of the BsNadR mutants (Figure S5A). The analysis of root mean square fluctuation (RMSF) suggested that AF11, AH6, and AB8 exhibited high, medium, and low flexibility in the DBD, respectively (Figure 3C). In concordance with their

https://doi.org/10.1021/acssynbio.1c00642
ACS Synth. Biol. 2022, 11, 1577−1587

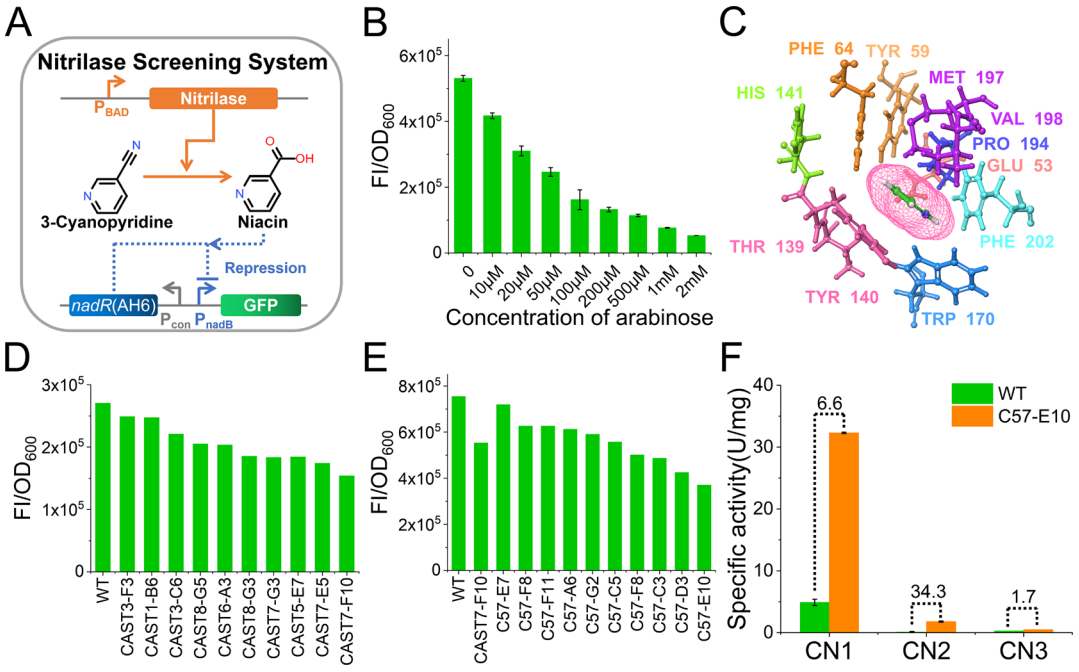

Figure 4. Construction and application of a high-throughput screening platform for nitrilase evolution. (A) Schematic diagram of the high-throughput screening system for nitrilase. The nitrilase expression cassette and NAsensor module were on two individual plasmids. Nitrilase was expressed under the control of the arabinose-inducible promoter P_{BAD}. The NAsensor with the mutant of AH6 sensed the niacin produced by nitrilase from 3-cyanopyridine. (B) Correlation between the concentration of arabinose and the GFP expression for the nitrilase screening system. (C) Residues that comprise the catalytic pocket of Nit6803. The residues used for site mutation in different groups were shown in different colors. (D) Screening of positive mutants from the library of each group. 50 μM of arabinose was added to induce the expression of Nit6803. (E) Screening of positive mutants through multi-site combinations of random saturation mutations. 20 μM of arabinose was added to induce the expression of Nit6803. (F) Determination of the specific activity of C57-E10 on various substrates. CN1, 3-cyanopyridine; CN2, 2-cyanopyridine; and CN3, benzonitrile.

repression on GFP expression, the results indicated that proper flexibility facilitated the binding of BsNadR to DNA, whereas too much rigidity prevented, as the similar phenomenons reported in various DNA-binding proteins.[34−36] A similar trend in flexibility was also observed in the EBD, which indicated that proper flexibility facilitated the binding of BsNadR to niacin. AF11 exhibited the highest affinity and the lowest binding free energy, whereas AB8 exhibited the lowest affinity and the highest binding free energy (Figure 3B,C). In addition, the volumes of the ligand-binding pocket of BsNadR during MD simulation were also calculated (Figure S5B). Overall, WT has the smallest volume of pocket. AF11, AH6, and AB8 have progressively larger pocket volumes (Figure S5C), which was consistent with their binding free energy to niacin. This result also provides a demonstration of the change in ligand-binding ability of the BsNadR mutants. Furthermore, the correlations of each residue were analyzed by the dynamics cross-correlation map (DCCM) (Figure S6). The differences in DCCM suggested the stronger association of EBD and DBD in BsNadR mutants than in WT. Moreover, among AF11, AH6, and AB8, AF11 has the strongest connection between EBD and DBD; AH6, moderate; and AB8, the weakest. The dynamical correlations between EBD and DBD of BsNadR mutants were consistent with their different regulatory properties.

The ligand-binding details of WT and three mutants were analyzed. As shown in Figure 3D, in the WT, a zinc ion formed a metal complex with Glu93, His152, and His154, which stabilized the ligand-binding pocket, and His85, His152, and His154 interacted with the carboxyl group *via* a salt bridge. Additionally, Phe132, Val107, and Ile121 were shown to be involved in hydrophobic interactions with the pyridine ring. The zinc ion complex and the salt bridge with the carboxyl group of niacin were completely retained in these mutants. By contrast, the binding of the pyridine ring with its interacting residues weakened considerably, especially in AH6 and AB8. The weakened binding resulted in an increase in binding free energy, which was consistent with the calculated results (Figure 3B).

High-Throughput Screening of Evolved Nitrilase by the NAsensor. The AH6 mutant accurately demonstrated the gradient GFP expression across 0−50 mM niacin, which is typically the product concentration range for enzyme activity assays. A high-throughput screening platform for nitrilase evolution was designed using AH6, and nitrilase from *Synechocystis* sp. PCC 6803 (Nit6803) was used to verify the validity of the system. As shown in Figure 4A, nitrilase is expressed under the control of the arabinose-inducible promoter P_{BAD}, which converts 3-cyanopyridine to niacin, eventually responding to the GFP expression level according to the converted niacin concentration. With increasing arabinose concentrations, a progressive decrease in the fluorescence intensity was observed, indicating that increasing arabinose concentrations resulted in elevated nitrilase expression and a higher concentration of niacin catalyzed from 3-cyanopyridine (Figure 4B). This result indicated that the platform could effectively reflect the intracellular activity of Nit6803.

A semi-rational directed evolution was designed based on CAST[37] to enhance the activity of Nit6803 using the constructed platform. The structure of Nit6803 with its

https://doi.org/10.1021/acssynbio.1c00642
ACS Synth. Biol. 2022, 11, 1577−1587

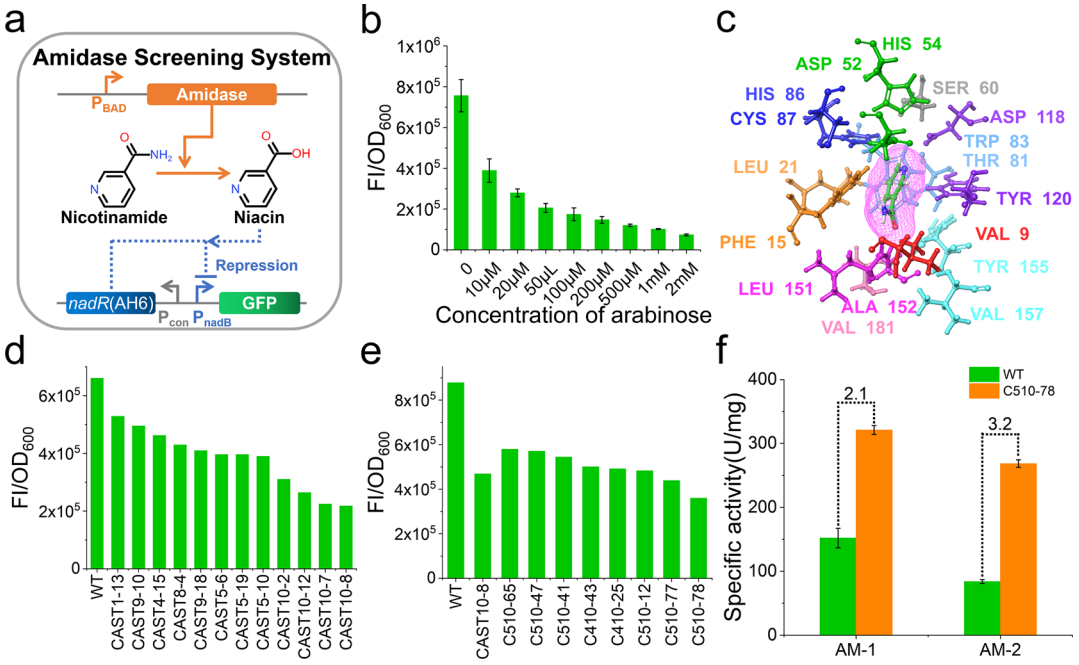

Figure 5. Construction and application of a high-throughput screening platform for amidase evolution. (A) Schematic diagram of the high-throughput screening system for amidase. The amidase expression cassette and the NAsensor module were on two individual plasmids. Amidase was expressed under the control of the arabinose inducible promoter P_{BAD}. (B) Correlation between the concentration of arabinose and the GFP expression for the nicotinamidase screening system. (C) Residues that comprise the catalytic pocket of EcPncA. The residues used for site mutation in different groups were shown in different colors. (D) Screening of positive mutants from the library of each group. 20 μM of arabinose was added to induce the expression of EcPncA. (E) Screening of positive mutants through multi-site combinations of random saturation mutations. 5 μM of arabinose was added to induce the expression of EcPncA. (F) Determination of the specific activity of C510-78 on various substrates. AM1, nicotinamide and AM2, pyrazinamide.

substrate 3-cyanopyridine was obtained using molecular docking (Figure S7), and the residues within 5 Å of the substrate, which were identified to form the catalytic pocket, were separated into eight groups (CAST1−CAST8), each containing one or two residues based on the distance in the sequence (Figure 4C). Eight site-saturated random mutant libraries were constructed, and the mutants in each library were identified using the screening platform. The transformants were pre-screened on the LB plate with 50 μM of arabinose and 20 mM of 3-cyanopyridine to exclude the inactive mutants. Then, the positive mutants were further verified in the 96-well plates and test tubes. The positive mutants that exhibited the most pronounced suppression of GFP expression were sorted out, and all of them were involved in CAST5 and CAST7 (Figure 4D). Subsequently, a combined saturation random mutagenesis of CAST5 and CAST7 was conducted. Positive mutants with multi-site combinations were screened by the screening platform using 20 μM arabinose and 20 mM 3-cyanopyridine (Figure 4E), and a mutant, C57-E10, exhibiting the most significant repression of GFP expression was isolated. C57-E10 was overexpressed, purified, and characterized. The specific activity of C57-E10 toward 3-cyanopyridine was found to be 6.6 times that of the WT (Figure 4F). In addition, the specific activity of C57-E10 toward 2-cyanopyridine and benzonitrile, the typical substrates used to determine nitrilase activity, was increased 34.3- and 1.7-fold, respectively (Figure 4F).

High-Throughput Screening of Evolved Amidase. A screening platform was constructed for amidase evolution using AH6 similar to that of nitrilase, where nicotinamide was converted to niacin by amidase and subsequently responded to the GFP expression level according to the converted niacin concentration (Figure 5A). Amidase from *E. coli* (EcPncA) was used as the target enzyme, and the availability of the platform was tested. With increasing arabinose concentrations, a progressive decrease in the fluorescence intensity was observed, demonstrating that increasing arabinose concentrations resulted in elevated EcPncA expression and subsequently a higher concentration of niacin was catalyzed from nicotinamide. This result indicated that the system could effectively reflect the intracellular activity of EcPncA (Figure 5B).

Similar to the evolution of nitrilase, a semi-rational directed evolution of EcPncA based on the CAST strategy was designed. The structure of EcPncA was established by homology modeling based on the crystal structure of amidase from *Acinetobacter baumannii* AYE[38] (PDB code: 2WT9, identity = 36.59%) (Figure S8). The catalytic pocket of EcPncA was determined using molecular docking (Figure S9), and residues within 5 Å of the substrate were assigned into 10 groups (CAST1−CAST10) (Figure 5C). Site-saturated random mutations were performed, and the positive mutants with improved activity were sorted out using 20 μM of arabinose and 20 mM of nicotinamide (Figure 5D). Then, combined saturation random mutagenesis was carried out, and the positive mutants were screened out using 5 μM of arabinose and 20 mM of nicotinamide (Figure 5E). The mutant of C510-78 exhibited the most significant repression of GFP expression when isolated (Figure 5E). The specific activity of the purified enzyme C510-78 showed a 2.1-fold increase over that of WT (Figure 5F). In addition to nicotinamide, another substrate that EcPncA can catalyze is

https://doi.org/10.1021/acssynbio.1c00642
ACS Synth. Biol. 2022, 11, 1577−1587

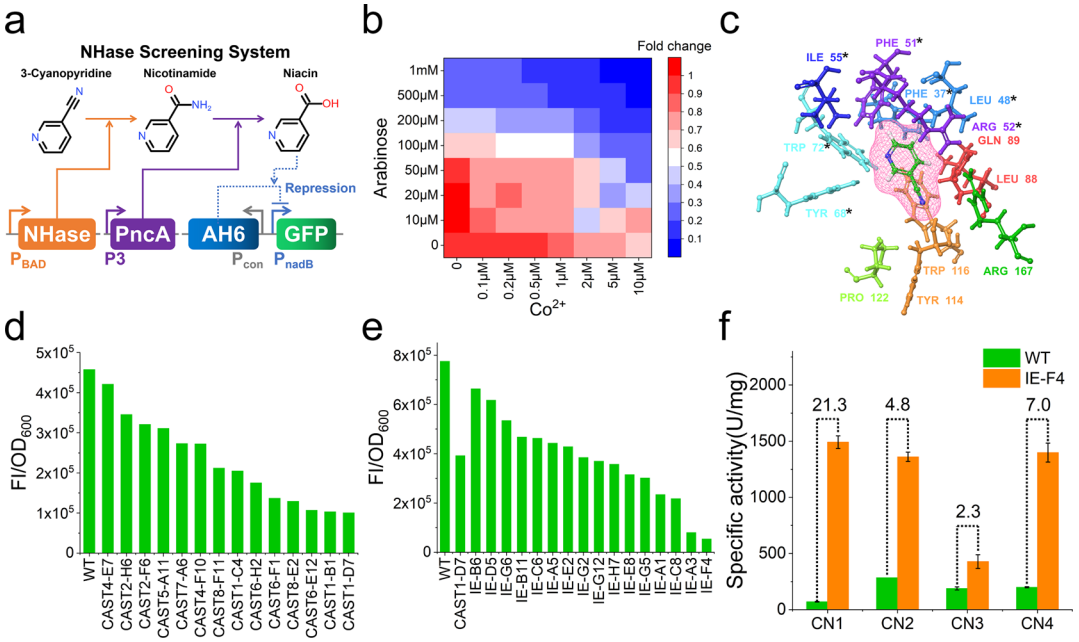

Figure 6. Construction and application of a high-throughput screening platform for NHase evolution. (A) Schematic diagram of the high-throughput screening system for NHase. A strong constitutive expression cassette of EcPncA was introduced into the NAsensor. (B) Influence of the concentration of arabinose and $CoCl_2$ on the fold change in the GFP expression for the NHase screening system. (C) Residues that comprise the catalytic pocket of PtNHase. The residues used for site mutation in different groups were shown in different colors. (D) Screening of positive mutants from the library of each group. The concentrations of arabinose and $CoCl_2$ were 100 and 1 μM, respectively. (E) Screening of positive mutants through multi-site combinations of random saturation mutations. The concentrations of arabinose and $CoCl_2$ were 20 and 1 μM, respectively. (F) Determination of the specific activity of IE-F4 on various substrates. CN1, 3-cyanopyridine; CN2, 2-cyanopyridine; CN3, benzonitrile; and CN4, 2-cyanopyrazine.

pyrazinamide, so we determined the activity of EcPncA on pyrazinamide. The result showed that the specific activity of C510-78 toward pyrazinamide was increased 3.2-fold (Figure 5F).

Directed Evolution of NHase through High-Throughput Screening Based on an Expanded NAsensor. The engineered mutant AH6 maintained the specificity of WT BsNadR, only responding to niacin but not 3-cyanopyridine and nicotinamide (Figure 2C). NHases can convert 3-cyanopyridine to nicotinamide, which could not be detected by the NAsensor. To develop a high-throughput screening platform for NHase evolution, a nicotinamide conversion module was introduced into the NAsensor, in which 3-cyanopyridine is converted to nicotinamide by NHase and then further converted to niacin by amidase. EcPncA was used as the amidase and overexpressed by the artificial strong constitutive promoter P3[39] and a strong ribosome-binding site, AAGGAG (Figure 6A). The expanded NAsensor responding to niacin and nicotinamide was verified. The signal outputs by the induction of niacin and nicotinamide were almost the same (Figure S10), which indicated that the nicotinamide added to the medium can be rapidly converted to niacin.

A thermostable NHase from *Pseudonocardia thermophila* JCM3095 (PtNHase)[40] was employed to evaluate the effectiveness of high-throughput screening of NHase. Compared to the low activity of nitrilase and amidase, PtNHase exhibited high activity, which easily resulted in full activation of the NAsensor. The cobalt ion concentration is known to affect the activity of PtNHase since the enzyme is a metalloenzyme that binds to cobalt ions in its active site.[25] Therefore, the intracellular PtNHase activity was regulated in two ways by controlling the concentration of either arabinose or cobalt ions. Based on these considerations, appropriate conditions for screening were determined under various concentrations of arabinose and cobalt ions. With an increase in arabinose and cobalt ion concentrations, the GFP expression was progressively suppressed, which established that the intracellular PtNHase activity could reflect the sensitivity of the NHase screening system (Figure 6B).

A CAST-based semi-rational directed evolution strategy was also applied to PtNHase. Residues forming the catalytic pocket were identified using molecular docking and assigned to nine groups (Figures 6C and S11). 14 positive mutants from each random saturation library were screened out using 100 μM arabinose, 1 μM $CoCl_2$, and 20 mM 3-cyanopyridine (Figure 6D). The best mutations were found in the groups of CAST1, CAST6, and CAST8, and CAST1-D7 exhibited the highest response. Subsequently, iterative evolution (IE) was performed by introducing random saturation mutations of CAST6 and CAST8 into CAST1-D7. As a result, the mutant IE-F4 that greatly suppressed GFP expression was isolated using 20 μM arabinose, 1 μM $CoCl_2$, and 20 mM 3-cyanopyridine (Figure 6E). The specific activity of IE-F4 toward 3-cyanopyridine was 21.3 times higher than that of the wild type (Figure 6F). Specific activities of IE-F4 toward 2-cyanopyridine, 2-cyanopyrazine, and benzonitrile, the typical substrates to determine the activity of NHase on aromatic substrates, were increased 4.8-, 7.0-, and 2.3-folds, respectively (Figure 6F).

Superiority of the High-Throughput *In Vivo* Screening System for Enzyme Evolution. Natural biosensors usually possess a narrow chemical concentration detecting range and an operating range, so the gradient signal output is difficult to achieve.[18−20] Although the ArgR- and VanR-based biosensors were applied for the screening of arginine deiminase

https://doi.org/10.1021/acssynbio.1c00642
ACS Synth. Biol. 2022, 11, 1577−1587

and tyramine oxidase, they can only detect products with a concentration less than 0.1 and 1 mM, respectively.[20,41] In this study, the NAsensor was adaptively evolved for a wider detection range of product concentration (0−50 mM), which aligns well with the range for the determination of enzyme activity. Moreover, the niacin dose-dependent gradient signal output makes the improved NAsensor capable of effectively distinguishing minor differences in enzyme activity. This study provided a paradigm for the development and application of other genetically coded biosensors.

For the reaction-then-assay screening platform,[8−10] additional reaction processes *in vitro* are necessary, which are inconvenient and costly. Biosensors can well couple enzyme activity and cell phenotypes, which enables enzymatic reaction and biosensor response to be performed sequentially in a single cell. Accordingly, the throughput of enzyme screening based on the NAsensor was greatly increased.

The evolution of three nitrile metabolism-related enzymes was successfully performed using the high-throughput *in vivo* automatic screening platform constructed in this study. Activities of these enzymes were dramatically improved similar to thosetoward other analogous substrates. Of course, we believe that there is still space for further activity enhancement *via* subsequent evolution by employing the high-throughput automatic screening platform. The NHase with enhanced activity has immense potential to promote the industrial production of acrylamide and nicotinamide, and the improved activities of nitrilase and amidase could enable the industrial application of these enzymes. For example, they may be utilized in the biosynthesis of amino acids from urea anhydrides and aminoamide.

METHODS

Strains, Plasmids, and Culture Conditions. *E. coli* JM109 cells were used as the host for the construction of the biosensor and the high-throughput screening system for enzymes. The chromosome of *B. subtilis* 168 was extracted and used as the template for cloning the BsNadR gene and promoters. The previously constructed plasmid pEV-GFP was used as the vector for the biosensor.[42] *E. coli* BL21(DE3) and the IPTG inducible vector pET24a(+) were used to overexpress the enzymes. The Luria−Bertani (LB; 10 g/L tryptone, 5 g/L yeast extract, 10 g/L NaCl, pH 7.0) medium was used for cell culture. When preparing the solid medium, 1.5% agar was added to LB. The antibiotics used for selection and culture were 50 μg/mL kanamycin and 50 μg/mL chloramphenicol. All the strains and plasmids used in this study have been listed in Table S1.

Genetic Manipulation. The seamless cloning technique based on Gibson assembly was used for plasmid construction. Gene and vector fragments were individually amplified using PCR with high-fidelity PrimeSTAR Max DNA Polymerase (Takara Bio Inc., Japan). Thereafter, the PCR products were treated with Dpn I (Takara Bio Inc., Japan) to remove the template and then cleaned up using the DNA Clean-up Kit (CWBIO, China). The purified fragments were seamlessly joined using the ABclonal MultiF Seamless Assembly Mix (ABclonal Technology Co. Ltd., China). The reaction product was directly transformed into *E. coli* JM109 competent cells. Finally, the transformed cells were plated onto an LB plate containing appropriate antibiotics. The primers used in this study are listed in Table S2. Homologous arms (20−30 bp) were designed into each primer for seamless ligation.

Desensitization Engineering of BsNadR Based on EP-PCR. EP-PCR was employed to introduce random mutations into BsNadR in order to generate mutants with various properties. First, EP-PCR was performed using the GeneMorph II Random Mutagenesis Kit (Agilent Technologies Inc., USA), with plasmid pEPnadB-GFP-nadR as the template. As per the manufacturer's instruction, the mutation frequency was set to medium (4.5−9 mutations/kb). Amplified fragments with random mutations were treated with DpnI to remove the template and then cleaned up. The purified fragments were seamlessly assembled onto the vector fragments and amplified using high-fidelity DNA polymerase with plasmid pEPnadB-GFP-nadR as the template. The assembled products were transformed into *E. coli* JM109 to construct the BsNadR mutant library.

To screen for the desensitized BsNadR, cells harboring BsNadR mutants were plated onto LB plates and cultured overnight at 37 °C. Highly fluorescent transformants, as observed by the naked eye under blue light, were inoculated into 96-well plates with or without 20 mM niacin. GFP expression was determined after incubation at 37 °C with shaking at 400 rpm for 24 h. Based on the fold change in repression of GFP expression by 20 mM niacin, the top 10 transformants were further verified in test tubes. They were first inoculated individually into test tubes containing 3 mL of LB and cultured at 37 °C with shaking at 200 rpm for 12 h. Thereafter, 100 μL of the culture fluid was transferred into a test tube containing 5 mL of LB, followed by incubation at 37 °C with shaking at 200 rpm for 24 h. The GFP expression was determined using the fluorescence intensity per OD_{600}. LB with 20 mM 3-cyanopyridine, 20 mM nicotinamide, or 20 mM niacin was utilized to set up experimental groups to verify the specificity of BsNadR mutants and LB without any additional function as the control.

High-Throughput Screening of Enzymes. The dual-plasmid high-throughput screening system was established to apply the NAsensor for automatic detection of *in vivo* enzyme activity. The biosensor module was placed in a vector harboring a high copy number of *ColE1* origin of replication and kanamycin resistance. The arabinose expression cassette was placed in the plasmid harboring a medium copy number of p15A origin of replication and chloramphenicol resistance. Thus, the expression levels of enzymes could be modulated by the addition of arabinose. The products obtained as a consequence of enzymatic catalysis of the substrate were subsequently detected using intracellular biosensors.

All enzymes included in this study underwent evolution using the CAST-based semi-rational strategy. Residues constituting the catalytic pocket were assigned to different groups according to their distance in the sequence. Each group included no more than two residues to minimize the number of potential mutants. The grouping information is listed in Table S4. This facilitated the scanning of hotspots for improvements in enzyme activity. Random saturation mutations were introduced into target sites by whole plasmid PCR using primers with the degenerate codon "NNK." The mutant library plasmid was constructed using the seamless assembly.

Screening of enzyme mutants was performed in three steps, namely, plate screening, 96-well plate screening, and further verification in test tubes. First, the products of seamless assembly harboring random saturation mutations were transformed into component cells with the appropriate biosensor. The transformants were plated onto LB plates with an

https://doi.org/10.1021/acssynbio.1c00642
ACS Synth. Biol. 2022, 11, 1577−1587

appropriate concentration of arabinose and 20 mM of the corresponding substrates. For every CAST group and IE, more than 4000 transformants were generated to cover all possible mutants as much as possible. Post incubation, fluorescence from single colonies was directly visible under blue light and provided an approximate estimation of the activity of the mutant enzymes. The transformants demonstrating weaker fluorescence than that of the wild type were inoculated into 96-well plates containing 600 μL of LB with appropriate concentrations of arabinose and the 20 mM substrate and were incubated at 37 °C with shaking at 400 rpm for 24 h. After determining the GFP expression, transformants with weaker fluorescence were transferred into test tubes containing 5 mL of LB with the arabinose and substrate and were incubated at 37 °C with shaking at 200 rpm for 24 h. Finally, the mutants were ranked according to the FI/OD_{600} values, and the mutants with the best performance were selected for sequencing and further analysis. The information of sequenced mutants of enzymes is listed in Table S5.

Fluorescence Assays. The cultured cells were harvested using centrifugation at 12,000*g* for 1 min and then washed thrice with phosphate-buffered saline (PBS; 8 g/L NaCl, 0.2 g/L KCl, 1.44 g/L Na_2HPO_4, and 0.24 g/L KH_2PO_4, pH 7.4). After being resuspended in PBS to make up the initial volume, 200 μL of cells were transferred into 96-well black-walled plates. The fluorescence intensity of GFP was determined using the Synergy H4 multimode microplate reader (excitation at 495 nm and emission at 525 nm). OD_{600} was measured simultaneously.

Overexpression, Purification, and Enzymatic Activity Assays. The IPTG-inducible vector pET24a(+) was used for the overexpression of the WT and mutant Nit6803, EcPncA, and PtNHase. When OD_{600} reached 0.6, IPTG was added to induce gene expression and the induction temperature was set at 25 °C to facilitate soluble expression of the enzymes. For EcPncA and PtNHase expression, 2 mM $ZnCl_2$ and 0.4 mM $CoCl_2$, respectively, were added.

The AKTA purifier (GE Healthcare UK Ltd., UK) was used for the purification of enzymes. The 6× His-tag was fused to the C-terminus to aid the purification of Nit6803 and EcPncA. A HisTrap HP 5 mL column (GE Healthcare UK Ltd.) equilibrated with binding buffer (20 mM Na_3PO_4, 0.5 M NaCl, and 5 mM imidazole, pH 7.4) was used to purify the 6× His-tagged protein. The bound proteins were eluted using elution buffer (20 mM Na_3PO_4, 0.5 M NaCl, and 0.5 M imidazole, pH 7.4). The active fractions were collected, concentrated using ultrafiltration, and dialyzed. Purification of PtNHase using Strep-tag was performed as described previously.[43] The concentration of enzyme was quantified by the Bradford method, and the purity was evaluated by SDS-PAGE.

To measure the specific activity of enzymes, a 500 μL reaction mixture comprising 10 μL of the enzyme and 490 μL of the substrate was set up. The reactions involving Nit6803 and EcPncA were conducted at 37 °C, and those for PtNHase were performed at 25 °C. Reactions were terminated by adding 500 μL of acetonitrile. High-performance liquid chromatography was employed to quantitate the products[43] (Figure S12). One unit (U) was defined as the amount of enzyme that produced 1 μmol of the product per minute. The concentrations of substrates for the enzymatic reaction were as follows: 200 mM 3-cyanopyridine; 200 mM 2-cyanopyridine; 100 mM 2-cyanopyrazine; 50 mM benzonitrile; 200 mM nicotinamide; and 100 mM pyrazinamide.

Homology Modeling. The structural analysis of Nit6803 and PtNHase was performed using the previously reported crystal structures 3WUY and 1IRE, respectively. The structures of BsNadR and EcPncA were constructed by homology modeling using the structures of their homologous proteins, NiaR from *Bacillus halodurans* (PDB code: 7CV2)[44] and PncA from *A. baumannii* AYE (PDB code: 2WT9),[38] as the template. Homology modeling was carried out using Schrödinger software, and the quality of built structures was confirmed using PyRAMA, a Python3 implementation of the Ramachandran plot (https://github.com/gerdos/PyRAMA).

Molecular Docking. Molecular docking was performed using the Glide module of the Schrödinger software in extra precision mode. The 3D structures of ligands or substrates were obtained from the PubChem database (https://pubchem.ncbi.nlm.nih.gov/) and subsequently pre-processed and optimized using the Schrödinger software. Fifty positions were generated in each docking, and the appropriate poses for further analyses were selected according to the docking scores and visual judgment. The interaction between the ligand/substrate and protein was analyzed using the web tool PLIP (https://plip-tool.biotec.tu-dresden.de/plip-web/plip/index).[45]

MD Simulations. NAMD 2.14 was used for all MD simulations with the CHARMM36 force field.[46] All input files for MD simulations were generated using the web tool CHARMM-GUI (https://charmm-gui.org/).[47] The CHARMM topology and parameter files for ligands were generated using CGenFF.[48] In MD simulation, the protein−ligand complex was solvated in a rectangular TIP3 explicit solvent box using 10 Å as the edge distance, and the system was neutralized by the addition of 0.15 M K^+ and Cl^-. A 2 fs time step, a cutoff of 12 Å for non-bonded interactions, periodic boundary conditions, and particle mesh Ewald were applied in MD simulation. The whole MD simulation included 1 ns of water equilibration under the *NVT* ensemble at 303.15 K and 20 ns of classical MD simulation under the *NPT* ensemble at 303.15 K. The root mean square deviation, RMSF, and DCCM of each simulation were analyzed using Bio3D.[49]

Binding Free Energy Calculation. In this study, all binding free energy calculations were performed using the FEP/HREMD method.[33] The input files for FEP/HREMD were generated using CHARMM-GUI.[50] Calculation was performed with NAMD 2.14 in a rectangular TIP3 explicit solvent box with 10 Å as the edge distance, in which 0.15 M K^+ and Cl^- were placed using the Monte Carlo method.

Calculation of the Pocket Volume. POVME 3.0 was used to determine the volume of the ligand-binding pocket.[51] Grid spacing and distance cutoff were set as 1.0 and 1.09, respectively. The pocket was defined in all grid points within 3 Å of the ligand. The pdb file containing 100 frames, extracted in 0.2 ns intervals from the trajectory file of a 20 ns MD simulation, was used as the input file for POVME 3.0. Finally, the results of all frames are averaged, and the standard deviation is calculated.

DATA AVAILABILITY

All data included in this study are available upon request by contact with the corresponding author.

https://doi.org/10.1021/acssynbio.1c00642
ACS Synth. Biol. 2022, 11, 1577−1587

■ ASSOCIATED CONTENT

Supporting Information

The Supporting Information is available free of charge at https://pubs.acs.org/doi/10.1021/acssynbio.1c00642.

Homology modeling of proteins; molecular docking analysis; MD simulation and related analysis of BsNadR; and chromatograms of HPLC (PDF)

■ AUTHOR INFORMATION

Corresponding Author

Zhemin Zhou − *School of Biotechnology, Jiangnan University, Wuxi, Jiangsu 214122, China;* orcid.org/0000-0003-0604-1885; Email: zhmzhou@jiangnan.edu.cn

Authors

Laichuang Han − *School of Biotechnology, Jiangnan University, Wuxi, Jiangsu 214122, China;* orcid.org/0000-0001-5224-6406

Xinyue Liu − *School of Biotechnology, Jiangnan University, Wuxi, Jiangsu 214122, China*

Zhongyi Cheng − *School of Biotechnology, Jiangnan University, Wuxi, Jiangsu 214122, China;* orcid.org/0000-0001-6825-5374

Wenjing Cui − *School of Biotechnology, Jiangnan University, Wuxi, Jiangsu 214122, China;* orcid.org/0000-0001-8760-3514

Junling Guo − *School of Biotechnology, Jiangnan University, Wuxi, Jiangsu 214122, China;* orcid.org/0000-0003-4083-8855

Jian Yin − *School of Biotechnology, Jiangnan University, Wuxi, Jiangsu 214122, China;* orcid.org/0000-0002-2284-1666

Complete contact information is available at: https://pubs.acs.org/10.1021/acssynbio.1c00642

Author Contributions

L.H. and Z.Z. conceived the project and wrote the paper. L.H., X.L., Z.C., W.C., and J.G. designed and performed all the experiments. L.H., X.L., and J.Y. analyzed the results.

Notes

The authors declare no competing financial interest.

■ ACKNOWLEDGMENTS

This work is supported by the Natural Sciences Foundation of Jiangsu (BK20210470), the China Postdoctoral Science Foundation (2021M701461), the International S&T Innovation Cooperation Key Project (2017YFE0129600), the Priority Academic Program Development of Jiangsu Higher Education Institutions, the 111 Project (no. 111-2-06), the Jiangsu Province "Collaborative Innovation Center for Advanced Industrial Fermentation" Industry Development Program, and the First-Class Discipline Program of Light Industry Technology and Engineering (LITE2018-04).

■ REFERENCES

(1) Zeymer, C.; Hilvert, D. Directed Evolution of Protein Catalysts. *Annu. Rev. Biochem.* **2018**, *87*, 131−157.

(2) Cao, Y.; Li, X.; Ge, J. Enzyme Catalyst Engineering toward the Integration of Biocatalysis and Chemocatalysis. *Trends Biotechnol.* **2021**, *39*, 1173−1183.

(3) Otten, R.; Pádua, R. A. P.; Bunzel, H. A.; Nguyen, V.; Pitsawong, W.; Patterson, M.; Sui, S.; Perry, S. L.; Cohen, A. E.; Hilvert, D.; Kern, D. How directed evolution reshapes the energy landscape in an enzyme to boost catalysis. *Science* **2020**, *370*, 1442−1446.

(4) Bunzel, H. A.; Anderson, J. L. R.; Hilvert, D.; Arcus, V. L.; van der Kamp, M. W.; Mulholland, A. J. Evolution of dynamical networks enhances catalysis in a designer enzyme. *Nat. Chem.* **2021**, *13*, 1017−1022.

(5) Yang, H.; Swartz, A. M.; Park, H. J.; Srivastava, P.; Ellis-Guardiola, K.; Upp, D. M.; Lee, G.; Belsare, K.; Gu, Y.; Zhang, C.; Moellering, R. E.; Lewis, J. C. Evolving artificial metalloenzymes *via* random mutagenesis. *Nat. Chem.* **2018**, *10*, 318−324.

(6) Druteika, G.; Sadauskas, M.; Malunavicius, V.; Lastauskiene, E.; Taujenis, L.; Gegeckas, A.; Gudiukaite, R. Development of a new Geobacillus lipase variant GDlip43 via directed evolution leading to identification of new activity-regulating amino acids. *Int. J. Biol. Macromol.* **2020**, *151*, 1194−1204.

(7) Belsare, K. D.; Andorfer, M. C.; Cardenas, F. S.; Chael, J. R.; Park, H. J.; Lewis, J. C. A Simple Combinatorial Codon Mutagenesis Method for Targeted Protein Engineering. *ACS Synth. Biol.* **2017**, *6*, 416−420.

(8) Si, T.; Li, B.; Comi, T. J.; Wu, Y.; Hu, P.; Wu, Y.; Min, Y.; Mitchell, D. A.; Zhao, H.; Sweedler, J. V. Profiling of Microbial Colonies for High-Throughput Engineering of Multistep Enzymatic Reactions *via* Optically Guided Matrix-Assisted Laser Desorption/Ionization Mass Spectrometry. *J. Am. Chem. Soc.* **2017**, *139*, 12466−12473.

(9) Qiao, Y.; Hu, R.; Chen, D.; Wang, L.; Wang, Z.; Yu, H.; Fu, Y.; Li, C.; Dong, Z.; Weng, Y.-X.; Du, W. Fluorescence-activated droplet sorting of PET degrading microorganisms. *J. Hazard Mater.* **2022**, *424*, 127417.

(10) Qiu, X.; Xu, P.; Zhao, X.; Du, G.; Zhang, J.; Li, J. Combining genetically-encoded biosensors with high throughput strain screening to maximize erythritol production in *Yarrowia lipolytica*. *Metab. Eng.* **2020**, *60*, 66−76.

(11) Markel, U.; Essani, K. D.; Besirlioglu, V.; Schiffels, J.; Streit, W. R.; Schwaneberg, U. Advances in ultrahigh-throughput screening for directed enzyme evolution. *Chem. Soc. Rev.* **2020**, *49*, 233−262.

(12) Ding, N.; Zhou, S.; Deng, Y. Transcription-Factor-based Biosensor Engineering for Applications in Synthetic Biology. *ACS Synth. Biol.* **2021**, *10*, 911−922.

(13) Yeom, S.-J.; Kim, M.; Kwon, K. K.; Fu, Y.; Rha, E.; Park, S.-H.; Lee, H.; Kim, H.; Lee, D.-H.; Kim, D.-M.; Lee, S.-G. A synthetic microbial biosensor for high-throughput screening of lactam biocatalysts. *Nat. Commun.* **2018**, *9*, 5053.

(14) Zhou, S.; Yuan, S.-F.; Nair, P. H.; Alper, H. S.; Deng, Y.; Zhou, J. Development of a growth coupled and multi-layered dynamic regulation network balancing malonyl-CoA node to enhance (2S)-naringenin biosynthesis in *Escherichia coli*. *Metab. Eng.* **2021**, *67*, 41−52.

(15) Zhao, N.; Song, J.; Zhang, H.; Lin, Y.; Han, S.; Huang, Y.; Zheng, S. Development of a Transcription Factor-Based Diamine Biosensor in *Corynebacterium glutamicum*. *ACS Synth. Biol.* **2021**, *10*, 3074.

(16) Jayaraman, P.; Holowko, M. B.; Yeoh, J. W.; Lim, S.; Poh, C. L. Repurposing a Two-Component System-Based Biosensor for the Killing of *Vibrio cholerae*. *ACS Synth. Biol.* **2017**, *6*, 1403−1415.

(17) Snoek, T.; Chaberski, E. K.; Ambri, F.; Kol, S.; Bjørn, S. P.; Pang, B.; Barajas, J. F.; Welner, D. H.; Jensen, M. K.; Keasling, J. D. Evolution-guided engineering of small-molecule biosensors. *Nucleic Acids Res.* **2020**, *48*, No. e3.

(18) Kunjapur, A. M.; Prather, K. L. J. Development of a Vanillate Biosensor for the Vanillin Biosynthesis Pathway in *E. coli*. *ACS Synth. Biol.* **2019**, *8*, 1958−1967.

(19) Hanko, E. K. R.; Paiva, A. C.; Jonczyk, M.; Abbott, M.; Minton, N. P.; Malys, N. A genome-wide approach for identification and characterisation of metabolite-inducible systems. *Nat. Commun.* **2020**, *11*, 1213.

(20) Yao, J.; He, Y.; Su, N.; Bharath, S. R.; Tao, Y.; Jin, J.-M.; Chen, W.; Song, H.; Tang, S.-Y. Developing a highly efficient hydroxytyrosol

whole-cell catalyst by de-bottlenecking rate-limiting steps. *Nat. Commun.* **2020**, *11*, 1515.
(21) Rodionov, D. A.; Li, X.; Rodionova, I. A.; Yang, C.; Sorci, L.; Dervyn, E.; Martynowski, D.; Zhang, H.; Gelfand, M. S.; Osterman, A. L. Transcriptional regulation of NAD metabolism in bacteria: genomic reconstruction of NiaR (YrxA) regulon. *Nucleic Acids Res.* **2008**, *36*, 2032−2046.
(22) Rossolillo, P.; Marinoni, I.; Galli, E.; Colosimo, A.; Albertini, A. M. YrxA is the transcriptional regulator that represses de novo NAD biosynthesis in *Bacillus subtilis*. *J. Bacteriol.* **2005**, *187*, 7155−7160.
(23) Wu, Z.; Liu, C.; Zhang, Z.; Zheng, R.; Zheng, Y. Amidase as a versatile tool in amide-bond cleavage: From molecular features to biotechnological applications. *Biotechnol. Adv.* **2020**, *43*, 107574.
(24) Gong, J.-S.; Shi, J.-S.; Lu, Z.-M.; Li, H.; Zhou, Z.-M.; Xu, Z.-H. Nitrile-converting enzymes as a tool to improve biocatalysis in organic synthesis: recent insights and promises. *Crit. Rev. Biotechnol.* **2017**, *37*, 69−81.
(25) Cheng, Z.; Xia, Y.; Zhou, Z. Recent Advances and Promises in Nitrile Hydratase: From Mechanism to Industrial Applications. *Front. Bioeng. Biotechnol.* **2020**, *8*, 352.
(26) Banerjee, A.; Sharma, R.; Banerjee, U. C. A rapid and sensitive fluorometric assay method for the determination of nitrilase activity. *Biotechnol. Appl. Biochem.* **2003**, *37*, 289.
(27) Black, G. W.; Brown, N. L.; Perry, J. J. B.; Randall, P. D.; Turnbull, G.; Zhang, M. A high-throughput screening method for determining the substrate scope of nitrilases. *Chem. Commun.* **2015**, *51*, 2660−2662.
(28) He, Y.-C.; Ma, C.-L.; Xu, J.-H.; Zhou, L. A high-throughput screening strategy for nitrile-hydrolyzing enzymes based on ferric hydroxamate spectrophotometry. *Appl. Microbiol. Biotechnol.* **2011**, *89*, 817−823.
(29) Banerjee, A.; Kaul, P.; Sharma, R.; Banerjee, U. C. A high-throughput amenable colorimetric assay for enantioselective screening of nitrilase-producing microorganisms using pH sensitive indicators. *J. Biomol. Screen* **2003**, *8*, 559−565.
(30) Bervoets, I.; Van Brempt, M.; Van Nerom, K.; Van Hove, B.; Maertens, J.; De Mey, M.; Charlier, D. A sigma factor toolbox for orthogonal gene expression in *Escherichia coli*. *Nucleic Acids Res.* **2018**, *46*, 2133−2144.
(31) He, X.; Chen, Y.; Liang, Q.; Qi, Q. Autoinduced AND Gate Controls Metabolic Pathway Dynamically in Response to Microbial Communities and Cell Physiological State. *ACS Synth. Biol.* **2017**, *6*, 463−470.
(32) Trivedi, V. D.; Mohan, K.; Chappell, T. C.; Mays, Z. J. S.; Nair, N. U. Cheating the Cheater: Suppressing False-Positive Enrichment during Biosensor-Guided Biocatalyst Engineering. *ACS Synth. Biol.* **2022**, *11*, 420−429.
(33) Jiang, W.; Thirman, J.; Jo, S.; Roux, B. Reduced Free Energy Perturbation/Hamiltonian Replica Exchange Molecular Dynamics Method with Unbiased Alchemical Thermodynamic Axis. *J. Phys. Chem. B* **2018**, *122*, 9435−9442.
(34) Feng, N.; Feng, H.; Wang, S.; Punekar, A. S.; Ladenstein, R.; Wang, D.-C.; Zhang, Q.; Ding, J.; Liu, W. Structures of heat shock factor trimers bound to DNA. *iScience* **2021**, *24*, 102951.
(35) Schmidl, S. R.; Ekness, F.; Sofjan, K.; Daeffler, K. N.-M.; Brink, K. R.; Landry, B. P.; Gerhardt, K. P.; Dyulgyarov, N.; Sheth, R. U.; Tabor, J. J. Rewiring bacterial two-component systems by modular DNA-binding domain swapping. *Nat. Chem. Biol.* **2019**, *15*, 690−698.
(36) Brown, C.; Campos-León, K.; Strickland, M.; Williams, C.; Fairweather, V.; Brady, R. L.; Crump, M. P.; Gaston, K. Protein flexibility directs DNA recognition by the papillomavirus E2 proteins. *Nucleic Acids Res.* **2011**, *39*, 2969−2980.
(37) Reetz, M. T.; Bocola, M.; Carballeira, J. D.; Zha, D.; Vogel, A. Expanding the range of substrate acceptance of enzymes: combinatorial active-site saturation test. *Angew. Chem., Int. Ed.* **2005**, *44*, 4192−4196.
(38) Fyfe, P. K.; Rao, V. A.; Zemla, A.; Cameron, S.; Hunter, W. N. Specificity and mechanism of Acinetobacter baumanii nicotinamidase: implications for activation of the front-line tuberculosis drug pyrazinamide. *Angew. Chem., Int. Ed.* **2009**, *48*, 9176−9179.
(39) Mutalik, V. K.; Guimaraes, J. C.; Cambray, G.; Lam, C.; Christoffersen, M. J.; Mai, Q.-A.; Tran, A. B.; Paull, M.; Keasling, J. D.; Arkin, A. P.; Endy, D. Precise and reliable gene expression via standard transcription and translation initiation elements. *Nat. Methods* **2013**, *10*, 354−360.
(40) Cheng, Z.; Lan, Y.; Guo, J.; Ma, D.; Jiang, S.; Lai, Q.; Zhou, Z.; Peplowski, L. Computational Design of Nitrile Hydratase from *Pseudonocardia thermophila* JCM3095 for Improved Thermostability. *Molecules* **2020**, *25*, 4806.
(41) Cheng, F.; Kardashliev, T.; Pitzler, C.; Shehzad, A.; Lue, H.; Bernhagen, J.; Zhu, L.; Schwaneberg, U. A Competitive Flow Cytometry Screening System for Directed Evolution of Therapeutic Enzyme. *ACS Synth. Biol.* **2015**, *4*, 768−775.
(42) Han, L.; Cui, W.; Lin, Q.; Chen, Q.; Suo, F.; Ma, K.; Wang, Y.; Hao, W.; Cheng, Z.; Zhou, Z. Efficient Overproduction of Active Nitrile Hydratase by Coupling Expression Induction and Enzyme Maturation *via* Programming a Controllable Cobalt-Responsive Gene Circuit. *Front. Bioeng. Biotechnol.* **2020**, *8*, 193.
(43) Cheng, Z.; Jiang, S.; Zhou, Z. Substrate access tunnel engineering for improving the catalytic activity of a thermophilic nitrile hydratase toward pyridine and pyrazine nitriles. *Biochem. Biophys. Res. Commun.* **2021**, *575*, 8−13.
(44) Lee, D. W.; Park, Y. W.; Lee, M. Y.; Jeong, K. H.; Lee, J. Y. Structural analysis and insight into effector binding of the niacin-responsive repressor NiaR from *Bacillus halodurans*. *Sci. Rep.* **2020**, *10*, 21039.
(45) Adasme, M. F.; Linnemann, K. L.; Bolz, S. N.; Kaiser, F.; Salentin, S.; Haupt, V. J.; Schroeder, M. PLIP 2021: expanding the scope of the protein-ligand interaction profiler to DNA and RNA. *Nucleic Acids Res.* **2021**, *49*, W530−w534.
(46) Best, R. B.; Zhu, X.; Shim, J.; Lopes, P. E. M.; Mittal, J.; Feig, M.; Mackerell, A. D., Jr. Optimization of the additive CHARMM all-atom protein force field targeting improved sampling of the backbone φ, ψ and side-chain $\chi(1)$ and $\chi(2)$ dihedral angles. *J. Chem. Theor. Comput.* **2012**, *8*, 3257−3273.
(47) Lee, J.; Cheng, X.; Swails, J. M.; Yeom, M. S.; Eastman, P. K.; Lemkul, J. A.; Wei, S.; Buckner, J.; Jeong, J. C.; Qi, Y.; Jo, S.; Pande, V. S.; Case, D. A.; Brooks, C. L., 3rd; MacKerell, A. D., Jr.; Klauda, J. B.; Im, W. CHARMM-GUI Input Generator for NAMD, GROMACS, AMBER, OpenMM, and CHARMM/OpenMM Simulations Using the CHARMM36 Additive Force Field. *J. Chem. Theor. Comput.* **2016**, *12*, 405−413.
(48) Vanommeslaeghe, K.; Raman, E. P.; MacKerell, A. D., Jr. Automation of the CHARMM General Force Field (CGenFF) II: assignment of bonded parameters and partial atomic charges. *J. Chem. Inf. Model.* **2012**, *52*, 3155−3168.
(49) Grant, B. J.; Skjærven, L.; Yao, X. Q. The Bio3D packages for structural bioinformatics. *Protein Sci.* **2021**, *30*, 20−30.
(50) Jo, S.; Jiang, W.; Lee, H. S.; Roux, B.; Im, W. CHARMM-GUI Ligand Binder for absolute binding free energy calculations and its application. *J. Chem. Inf. Model.* **2013**, *53*, 267−277.
(51) Wagner, J. R.; Sørensen, J.; Hensley, N.; Wong, C.; Zhu, C.; Perison, T.; Amaro, R. E. POVME 3.0: Software for Mapping Binding Pocket Flexibility. *J. Chem. Theor. Comput.* **2017**, *13*, 4584−4592.

https://doi.org/10.1021/acssynbio.1c00642
ACS Synth. Biol. 2022, 11, 1577−1587